ELSEVIER

Journal of Power Sources 79 (1999) 43–59

JOURNAL OF POWER SOURCES

Engineering aspects of the direct methanol fuel cell system

K. Scott *, W.M. Taama, P. Argyropoulos

Chemical and Process Engineering Department, University of Newcastle upon Tyne, Merz Court, Newcastle upon Tyne, NE1 7RU, UK

Received 6 November 1998; received in revised form 5 December 1998; accepted 5 December 1998

Abstract

The direct methanol fuel cell presents several interesting scientific and engineering problems. There are many engineering issues regarding eventual application concerning cell materials, feed and oxidant requirements, fuel utilisation and recovery, scale up, etc. This paper looks at several of these issues starting from the point of current, typical, cell performance. A small-scale flow cell and a large scale cell, both with a parallel channel flow bed design, are used. The structure of the direct methanol fuel cell (DMFC) is a composite of two porous electrocatalytic electrodes; Pt–Ru–C catalyst anode and Pt–C catalyst cathode, on either side of a solid polymer electrolyte (SPE) membrane. Flow visualisation on small scale and intermediate scale (100 cm^2) cells has been used in the design of a new large-scale cell of 225 cm^2 active area. We discuss several important engineering factors in the successful design of large scale DMFCs including the use of vapour and liquid feeds, thermal management, gas management, methanol fuel management, hydrodynamics and mass transport.

Keywords: Fuel cell; Direct methanol; Polymer electrolyte; Electrocatalysis; Platinum ruthenium; Engineering; Scale up

1. Introduction

Recent years has seen an upsurge in interest in fuel cells for a range of applications, including transport and smaller scale static power. This interest has been largely generated by the breakthroughs made in the application of solid polymer electrolyte fuel cells. This activity has mainly been directed at the use of hydrogen as the clean source of fuel. The use of hydrogen brings with it issues regarding the appropriate and safe transportation and storage of the fuel and several methods have been advocated and are being researched and developed. An alternative is to use a liquid fuel and to reform/oxidise this fuel to hydrogen in situ, which itself brings issues of cost and overall operation into to play. Consequently a cell which can utilise a liquid fuel directly, without reformation, is attractive and several fuels have been proposed and researched, including methanol, methoxymethanes, formic acid, methyl formate, ethanol, etc. A requirement of the fuel is that, on oxidation, a clean combustion to carbon dioxide is achieved, which limits the choice, with currently available electrocatalysts, to simple species such as methanol.

The direct methanol fuel cell (DMFC) uses methanol, either vapour or liquid, as fuel and operates at relatively low temperatures ($< 100°C$). The cell reactions are

$$\text{Anode side: } CH_3OH + H_2O \rightarrow 6e^- + 6H^+ + CO_2 \quad (1)$$

$$\text{Cathode side: } \frac{3}{2}O_2 + 6e^- + 6H^+ \rightarrow 3H_2O \quad (2)$$

which can be combined and give the overall reaction:

$$CH_3OH + \frac{3}{2}O_2 \rightarrow 2H_2O + CO_2 \quad (3)$$

Thus the overall cell reaction is the combustion of methanol to carbon dioxide and water. The structure of the DMFC is a composite of two porous electrocatalytic electrodes on either side of a solid polymer electrolyte (SPE) membrane. The thermodynamic reversible potential for the overall cell reaction is 1.214 V, which compares favourably to 1.23 V for the hydrogen fuel cell and, consequently has generated the interest in the DMFC as an alternative power source.

However a current advantage of the hydrogen cell, over the DMFC, is that hydrogen oxidation at the anode is very

* Corresponding author. Tel.: +44-191-2228771; Fax: +44-191-222-5292

0378-7753/99/$ - see front matter
PII: S0378-7753(98)00198-0

fast and consequently the performance of the hydrogen cell is better than that of the methanol cell. For methanol, six electrons must be exchanged for complete oxidation and consequently the oxidation kinetics are inherently slower, as a result of intermediates formed during methanol oxidation [1]. Oxidation of the intermediates to carbon dioxide requires the adsorption of an oxygen containing species (e.g., OH, H_2O). Adsorption of these species does not occur substantially until potentials well above open circuit values [2]. Platinum alone is not a sufficiently active methanol oxidation electrocatalyst and the promotion of methanol oxidation has been actively studied. Currently significant results have been achieved with the use of binary catalysts, notably Pt–Ru. With these catalysts the second metal forms a surface oxide in the potential range for methanol oxidation [3].

Developments in electrode fabrication techniques and better cell designs for vapour fed cells, have brought dramatic improvements in cell performance in small-scale DMFCs. Typically, power densities higher than 0.18 W cm^{-2} are achievable [4], and power densities higher than 0.3 W cm^{-2} have been reported [5]. A number of authors have reported performance data for liquid feed DMFCs, e.g., Ravikumar and Shukla [6], Surampudi et al. [7], Valdez et al. [8], and Narayanan et al. [5] Surampadi et al. [7] reported the performance of a DMFC with solid polymer electrolyte (Nafion®) using a supported Pt–Ru catalyst anode of unknown manufacture. The influence of temperature and methanol concentration was briefly reported. The performance of a small stack of 5 cells (25 cm^2 cross-section) at temperatures of less than 60°C has been reported [8]. The catalyst loading was 4 mg cm^{-2} of an in house produced Pt–Ru catalyst supported on carbon. Both pieces of research confirmed that higher temperatures produced higher cell power. Power densities between approximately 150 to 300 mW cm^{-2} have been reported for liquid feed DMFC using different fabrication procedures (mainly undisclosed) [8] These power densities, although commercially attractive, are substantially lower than those obtained with H_2 fuel cells, 0.6–0.7 W cm^{-2}, while platinum anode catalyst loading for the hydrogen cells can be substantially lower (0.1 mg Pt cm^{-2}).

In the future research and development of the DMFC and similar organic fed fuel cells, there are several issues which have to be addressed and include thermal management, gas management, methanol fuel management and hydrodynamics, and mass transport. In vapour feed DMFCs there is a substantial energy requirement to vaporise the aqueous based fuel. In operation, the production of carbon dioxide, from methanol oxidation, means that there is a major requirement to separate the unused fuel from the anode exhaust gas containing substantial quantities of carbon dioxide. These factors, together with potential problems in cell thermal management and water management, have focused attention on liquid feed direct methanol fuel cells (LFDMFC), where, in principle, the carbon dioxide is formed as a separate phase to the fuel. The carbon dioxide can then be simply disengaged from the liquid fuel using standard gas liquid separators. This however leads to further problems associated with fuel utilisation and recovery, which are discussed in this paper. In the LFDMFC, methanol is directly oxidised to carbon dioxide using fuel cell electrodes almost identical to those used for vapour fed operation, i.e., Nafion®/Teflon bonded Pt–Ru catalysts dispersed onto carbon. The overvoltages experienced at both electrodes in the DMFC lead to a significant reduction in cell voltage from the theoretical maximum and thus research has focused on efforts to minimise these overvoltages. Thus research in several institutions is exploring several areas: new proton conducting membranes with reduced methanol permeability but with high conductivity, new anode catalysts and structures, new cathode catalyst tolerable to the presence of methanol and new MEA fabrication procedures.

Methanol crossover [4] results in a mixed potential at the cathode with significant loss in oxygen reduction performance. Thus to improve the DMFC performance it is important to seek ways to reduce the extent of methanol crossover. Much of the research on SPE fuel cells systems has used Nafion®, from DuPont, or similar membranes, e.g., Flemion (Asahi). Alternative polymer membrane electrolytes which exhibit lower methanol permeation rates, e.g., polybenzimidazole [9] and perfluorinated sulphonimides [10] have been considered as a means of reducing the impact of methanol crossover, as have zeolites [11]. A membrane material (unidentified) with a significantly reduced crossover of methanol in comparison to Nafion® is reported [5]. We have recently reported [11] the performance of a direct methanol fuel cell using aqueous methanol feed with anode catalysts (Pt–Ru) of 2 mg cm^{-2}. The suggested optimum methanol concentration, that could be used without significant methanol crossover and loss in cell performance, is 2 mol dm^{-3}.

This paper discusses engineering issues associated with the use of liquid fed DMFCs and, in particular, the factor of carbon dioxide gas management and subsequent recovery of vaporised methanol from the cell exhaust gas. We report typical performance data using a small-scale cell and a large-scale cell, both with the same design of flow bed and internal flow manifold. We assess the performance requirements of liquid fed and vapour fed DMFCs in terms of thermal management, gas management and methanol fuel management.

2. Experimental

2.1. Small scale cells

Tests on the DMFC were performed with two cell designs.

(1) Small scale cell, cross-sectional area of 9 cm^2, shown schematically in Fig. 1a. The cells were fitted with a membrane electrode assembly (MEA) sandwiched between two graphite blocks with flow beds cut out for methanol and oxygen–air flow. The flow bed consisted of a series of 10 parallel channels, 2 mm deep by 2 mm wide every 1 mm. The cell was held together between two aluminium backing plates using a set of retaining bolts positioned around the periphery of the cell. Electrical heaters, supplied by Watson Marlow, were placed behind each of the graphite blocks in order to heat the cell to the desired operating temperature. The graphite blocks were also provided with electrical contacts and small holes to accommodate thermocouples. The fuel cells were used in a

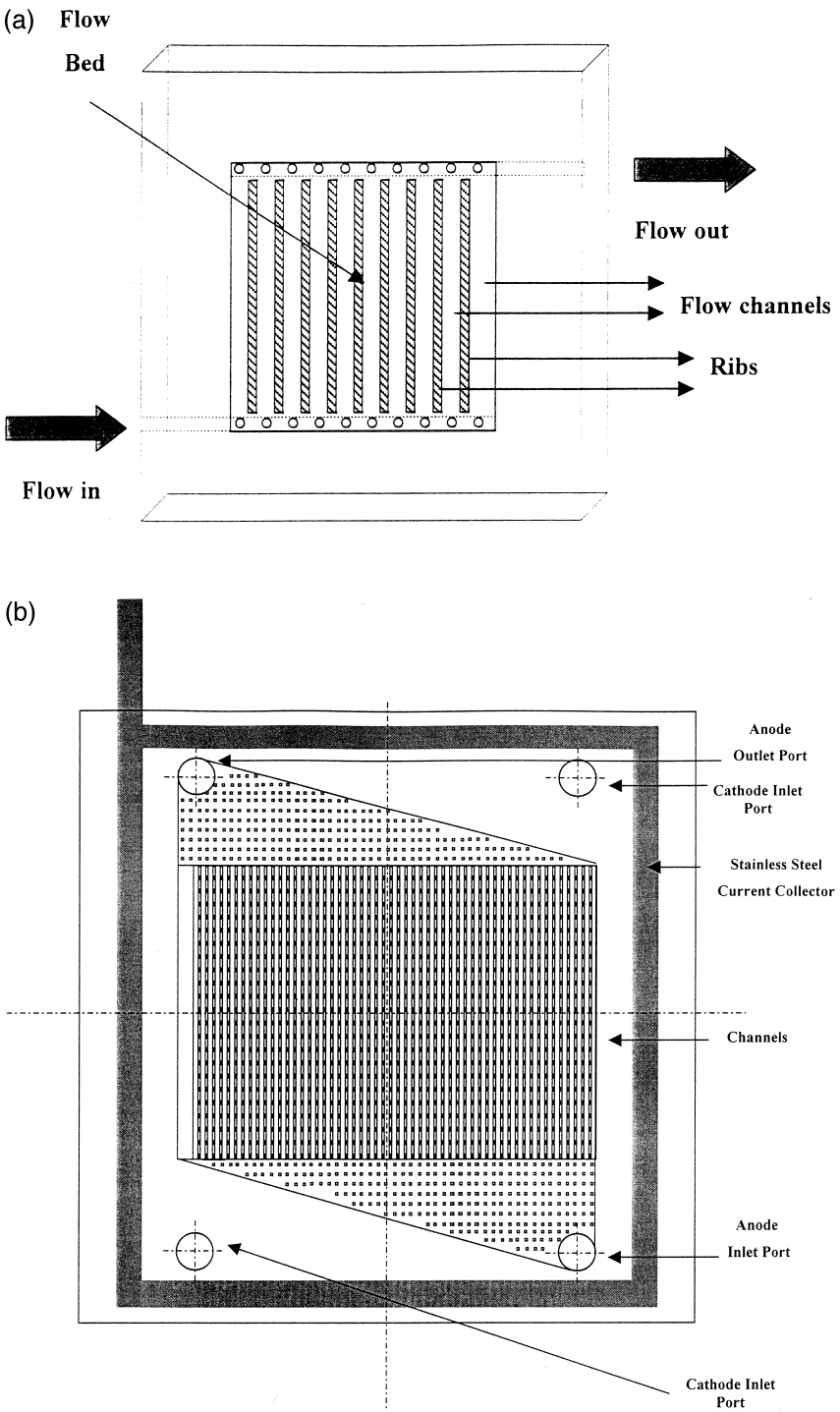

Fig. 1. Schematic diagrams of the experimental DMFCs. (a) Small scale cell. (b) Large flow visualisation cell.

simple flow rig, which consisted of a Watson Marlow peristaltic pump to supply aqueous methanol solution, from a reservoir, to a Eurotherm temperature controller to heat the methanol. Oxygen and air was supplied from cylinders at ambient temperature, and the pressure regulated at inlet by pressure regulating valves. All connections between the cells and equipment were with PTFE tubing, fittings and valves.

(2) The large-scale cell, active area of 204 cm^2, was based on the parallel channel design of the small cell. The channel dimensions were the same as that in the small cell and thus scale up was achieved by simply increasing the MEA cell cross-section. The cell was operated in a flow circuit, shown schematically in Fig. 2, which provided a controlled rate of fuel and oxidant flow. This circuit consisted of three pumps connected in parallel two peristaltic ones (Watson Marlow 505 U), and a centrifugal one (Totton Pumps with PVDF pump parts). A bypass loop with a control valve was used in order to control the flow rate of the centrifugal pump and a Platon Fmet series flow meter for measuring the flow rate. The maximum flow rate attainable from all three pumps is 6.0 l min^{-1}. The necessary heat load for the stack start-up and for replenishing the heat losses was provided by a Watlow 1.25 kW stainless steel heater controlled by an embedded thermocouple and an external PID temperature controller. Anode side exhaust gas and excess feed pass through a specially designed separation tank. Two dense layers of stainless steel mesh are used in order to achieve gas–liquid separation. The liquid flows downwards to the main reservoir when the gas is vented from the top of the column through a glass condenser, to recover vaporised methanol from carbon dioxide gas exhaust. A compressor supplies the required air quantity at the desired pressure for the cathode. A set of two Platon Fmet series flow meters with two precision valves is used to control the air supply. The cathode side exhaust gas is passed through a collection tank, to trap the water that separated from the air with the aid of a second condenser placed on the top of the vessel. At the top of the condenser there is a precision valve in order to control the cathodic compartment over-pressure. For cold start-up the necessary heat is provided with a pair of heating plates with embedded resistances. The plates were placed adjacent to the two end plate graphite blocks, and were supplied from a Farnel AR60-50 regulated power supply source, controlled with the aid of a computer.

MEAs studied in this work were made in the following manner. The anode consisted of a Teflonised (13%) carbon cloth support (E-Tek, type 'A') of 0.35 mm thickness, upon which was spread a thin layer of uncatalysed (ketjenblack 600) carbon bound with 10 wt.% Nafion® from a solution of 5 wt.% Nafion® dissolved in a mixture

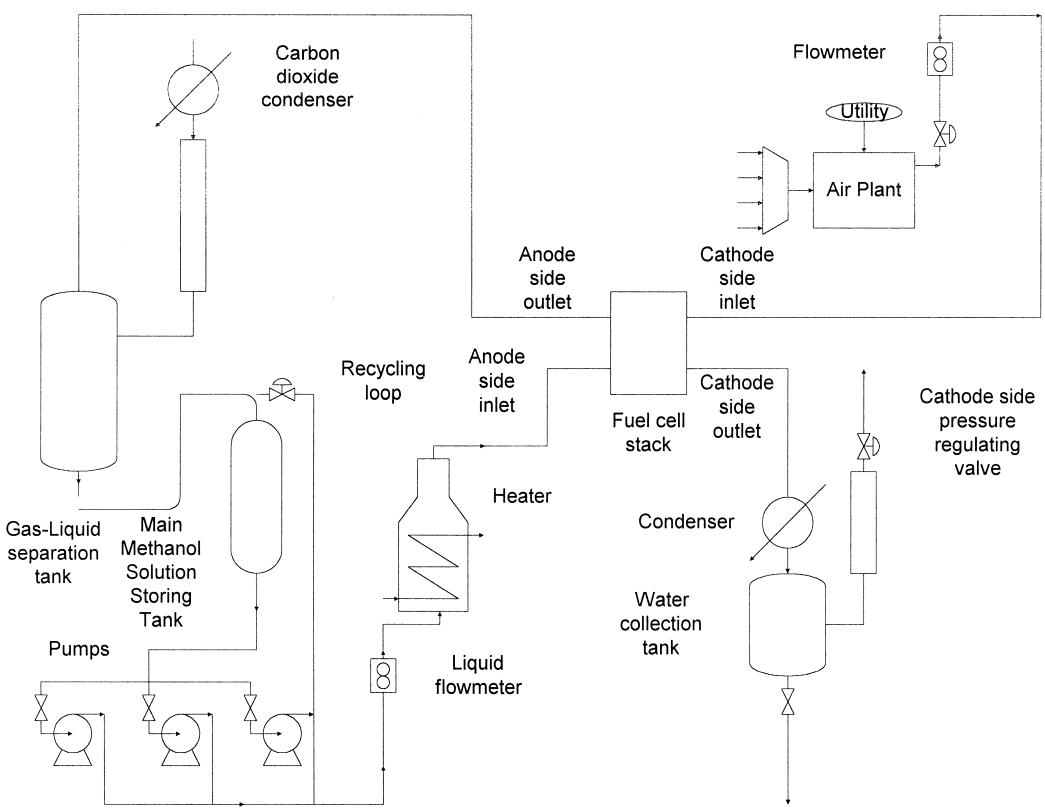

Fig. 2. Flow circuit for large-scale cell.

of water and lower aliphatic alcohol's (Aldrich™). The catalysed layer, Pt–Ru dispersed on carbon (2 mg cm^{-2} metal loading) and bound with 10 wt.% Nafion®, was spread on this diffusion backing layer. A thin layer of Nafion® solution was spread onto the surface of each electrode. The MEA was obtained by hot pressing the anode and cathode on either side of the pre-treated membrane. The thickness of the MEA is approximately 0.8 mm depending on the diffusion layer thickness.

The Pt–Ru anode catalyst used in this study were:

- Electrochem. (USA); Pt, 20 wt.%, Ru 10 wt.% on Vulcan XC-72R carbon
- Johnson Matthey (UK); 35 wt.% Pt, 15 wt.% Ru on Vulcan XC-72R carbon
- In house catalyst; 40 wt.% Pt, 20 wt.% Ru on ketjen black carbon.

The cathode was constructed using the same method as for the anode, a diffusion layer bound with 10 wt.% PTFE and a catalyst layer consisting of 10 wt.% Pt on carbon catalyst with a loading 1 mg cm^{-2} Pt black (Johnson Matthey) with 10 wt.% Nafion®. The electrodes were placed either side of a pre-treated Nafion® 117 membrane (Aldrich). This pre-treatment involved boiling the membrane for 1 h in 5 vol.% H_2O_2 and 1 h in 1 M H_2SO_4 before washing in boiling Millipore water (>18 mΩ) for 2 h with regular changes of water. The assembly was hot-pressed at 100 kg cm^{-2} for 3 min at 135°C. The resulting MEA was installed in the cell after pressing, and hydrated with water circulated over the anode at 75°C for 48 h. The majority of data reported here were obtained after allowing 48 h to condition a new MEA in the test fuel cell at 75°C and atmospheric pressure with continuous feed of 2 M methanol solution. Several MEAs were tested to ascertain reproducibility of the data.

Data are reported using the following standard conditions unless otherwise stated: methanol concentration: 2 mol dm^{-3}; methanol solution flow rate: 0.84 cm^3 min^{-1}; cell temperature: 90°C; anode catalyst: Electrochem.; air pressure: 2 bar.

2.2. Flow visualisation cells

Two cell designs were investigated in this study (see Fig. 1); a small scale cell with an active cross-sectional area of 9 cm^2, and a larger cell with an active cross-sectional area of 102 cm^2. The cells used were made from transparent acrylic, for the anode side and from graphite block, for the cathode side, and they were compression sealed with the aid of wet thread, teflon tape. The small cell had a set of ten parallel flow channels, 2 mm deep, 2 mm wide and 30 mm long machined into the acrylic block. The width of the ribs which formed the flow channels was 1 mm. Flow in and out of the cell was via a series of 2 mm diameter holes at the cell inlet and outlet which connected into a 10 mm diameter internal manifold.

The large cell, shown schematically in Fig. 1b, had a different flow bed design to that of the small cell. This design was a result of research on a large scale DMFC with a flow bed design and manifold arrangement identical to that of the small cell. The design is based on a compact heat exchanger, and is in three sections: a triangular enlarging inlet section, 30 mm long, which had a series of 4 mm^2 square spots, a central region of parallel flow channels of the cross-section as the small cell and a triangular, outlet section, of a similar design to the inlet section. Methanol solution supply to the cell is from a 6-mm diameter inlet at one corner at the bottom of the graphite plate and methanol solution and carbon dioxide gas leaves at the opposite corner at the top of the cell. The design of flow bed for the supply of air (or oxygen) is identical to that for the methanol (anode) side of the cell.

In both cells current was withdrawn using a peripheral stainless steel strip embedded into the acrylic block which contacted the MEA. A limitation with the arrangement is the relatively inefficient way of collecting the current produced (from the periphery with the aid of a stainless steel frame), which limited the cell current density to values below 100 mA cm^{-2} to minimise problems of current maldistribution.

In operation the cells were tested in a simple flow circuit with methanol solution supplied by two Watson Marlow 505U peristaltic pumps. The temperature control was achieved with, a variable voltage supply, an in-house electric heater and a Eurotherm temperature controller with an embedded thermocouple in the methanol solution tank. Air or oxygen gas was supplied from gas cylinders, and the pressure was controlled by a needle valve at the cell cathode side outlet.

The flow of methanol and carbon dioxide gas was recorded using a high speed Hitachi CCTV video camera (HV-720K). A stroboscope was placed behind the camera to provide the necessary lighting for the camera. The images were recorded in a video recorder, and then converted off-line to a computer image with the aid of Matrox PC card. An important issue in designing a DMFC is to ensure that there is a uniform distribution of liquid between all the flow channels, across the cell, to attain a uniform supply of methanol fuel to the MEA. This uniformity of flow was confirmed, over a range of flow rates, by observing the rise in liquid level in all channels.

3. Cell performance

Many parameters and variables affect the cell voltage, current density response of the DMFC including: temperature of fuel, methanol concentration, oxygen partial pressure, fuel and oxidant flows, the type of proton exchange membrane, catalyst preparation, the electrode structure and the cell design. In the small cells used in this research,

oxidant flows were significantly above stoichiometric requirements and did not influence performance.

Fig. 3 shows typical performance data for the small-scale cell, and illustrates the influence of temperature, air pressure and methanol concentration on cell voltage performance. The higher temperature and higher air pressure both give better performance with maximum power densities reaching nearly 100 mW cm^{-2}. Investigations of the effect of methanol concentration demonstrated that power density is a maximum at a concentrations of 2 mol dm^{-3} as previously reported by Ravikumar and Shukla [6]. A higher concentration of methanol does not lead to an improvement of cell power due to the derogatory effect of methanol crossover, from anode to cathode, through the membrane on the oxygen reduction reaction. Methanol is partially oxidised at the cathode and thus causes a mixed potential, reducing the cathode potential. At lower methanol concentrations of 0.5 mol dm^{-3} and below there is a significant reduction in the power performance and at higher current densities a sharp fall in cell voltage is observed, which is in part due to mass transfer limitations

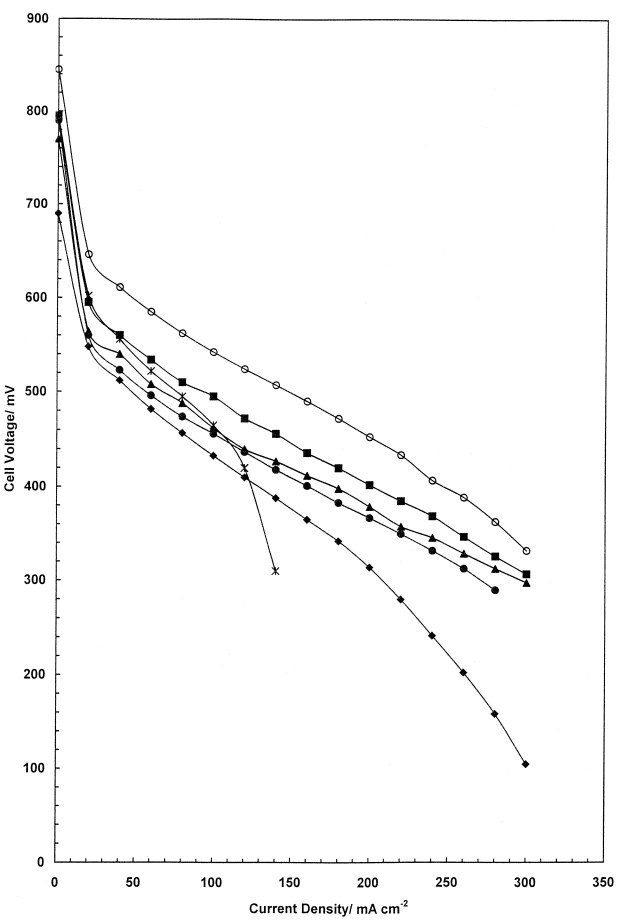

Fig. 3. Typical electrical performance of the small scale DMFC: the effect of temperature, air pressure and methanol concentration on the performance of the DMFC. ♦ 65°C, ■ 90°C, ▲ 0.05 bar air pressure, ○ 1.5 bar air pressure, * 0.5 M methanol, ● 2 M methanol.

of methanol in the MEA. Under the conditions used a limiting current of approximately 1600 A m^{-2} is observed with a 0.5 mol dm^{-3} methanol solution. Similar limiting current densities have been reported by Ravikumar and Shukla [6]. This current density is equivalent to a mass transport coefficient of 3.3×10^{-6} m s^{-1}.

The effect of mass transport on the performance of the DMFC can be quickly assessed from a preliminary mass transport calculation. If we consider that the carbon cloth backing layer is the only region imposing mass transport limitations by diffusion and that no convective flow occurs. The cloth thickness is around 280 μm. Then with a diffusion coefficient of 2.8 10^{-9} m^2 s^{-1} a mass transfer coefficient for the cloth is K_l = Diffusivity/thickness = $2.8 \times 10^{-9}/280\ 10^{-6} = 10^{-5}$ m s^{-1}.

The mass transport limiting current density for a cloth containing a volume fraction of liquid, e_l, is

$$j_l = 6FK_l e_l^{1.5} C_{\text{methanol}}, \quad (4)$$

For a 0.5 mol dm^{-3} methanol solution the limiting current density is

$$j_l = 6.96500 \times 10^{-5} e_l^{1.5} \cdot 500 \cong 3000 e_l^{1.5}\ \text{A m}^{-2}, \quad (5)$$

It is not possible to measure the volume fraction of methanol solution in the carbon cloth during operation. However, in the range of liquid volume fraction of 0.6 to 0.8, limiting current densities are between approximately 1400 to 2150 A m^{-2}. Thus, not surprisingly, mass transport limitations occur with relatively low concentrations of methanol researched in DMFC operation. In view of the fact that the product carbon dioxide gas must also escape from the electrode through the cloth and thus inhibit the mass transport of methanol limiting, currents are likely to be significantly lower than estimated above.

3.1. Large scale cell performance

Fig. 4 shows performance data for the large-scale cell operating at a temperature of 70°C, with 2 bar air with a flow rate of 800 cm^3 min^{-1} of 2 M methanol solution. It is apparent that although the open circuit voltage of the large-scale cell is comparable to that of the small-scale cell, the operating cell voltage performance is significantly different and inferior. For example, there is a typical 100 mV lower cell potential at a current density of 100 mA cm^{-2} for the large cell. The cell voltage response was not stable during operation and fluctuated continuously during the collection of the data. As the current density was increased, and thus gas evolution also increased, it was apparent that the anode outlet manifold could not deal with the large volume of gas produced and restricted the liquid flow. Presumably within the cell anode channels there were severe problems with gas flow and the formation of gas slugs under the conditions of operation used, which manifested itself into poor cell voltage performance. As a

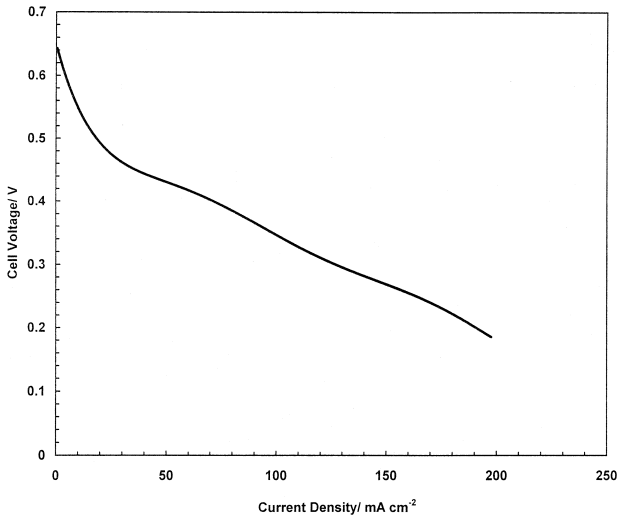

Fig. 4. Performance of the large scale cell (70°C, 800 ml min^{-1} anode side inlet flow rate, 2 bar air pressure).

consequence of this initial large-scale test we instigated a flow visualisation study to examine the gas flow, and flow bed and manifold design [12].

4. Flow visualisation studies

Following the relatively poor and unstable performance of the large simple parallel channel design we undertook a study of the gas evolution and flow in the anode side of the DMFC with a model small scale cell. Two different materials were studied in the small size cell: Toray (wet-proofed) carbon paper and E-TEK type 'A' carbon cloth. These two materials have a quite different structure. Carbon paper is formed by pressing carbon fibres and hence has a smaller porosity than the carbon cloth. The carbon cloth is a plain weave cloth.

Fig. 5 shows a view of operating MEAs, made with either carbon paper or carbon cloth, under exactly the same conditions (current density 30 mA cm^{-2}, channel flow rate 2.5 ml min^{-1} of the flow bed). As it can be seen the flow regime is different in the two cases. For the carbon paper MEA, large gas slugs are formed (0.8–1.8 mm) which tend to attach to the surface of the paper and block the channel. This is explained from the texture of the paper surface, which creates a different surface tension between the bubble and the surface and enhances friction between the bubbles or slugs and the material itself. In the long term (in that case after a few minutes) this leads to a complete blocking of all the flow bed channels accompanied by a rapid deterioration of the cell electrical performance. In the case of the cloth MEA the flow regime can be described as bubbly with relatively small gas bubbles (0.6–0.8 mm) formed which have a tendency to coalesce.

The manifold design used for the small cell is comprised of a straight circular cross-section tube machined inside the main body of the acrylic block, with holes open on its periphery. A problem with the flow distribution design is that the flow had to suddenly change orientation twice. Thus when gas slugs are produced which are larger than the hole cross-section they have to be forced through a hole, which is achieved either by compressing the gas or by breaking the slug into smaller gas bubbles. In addition the gas flow has to overcome the friction and two-phase flow related pressure drop in the outlet manifold and the exterior flow loop. At low flow rates this is difficult to achieve and only happens when there is an excessive amount of gas trapped inside the cell and the manifold. There are thus instances when all the outlet manifold

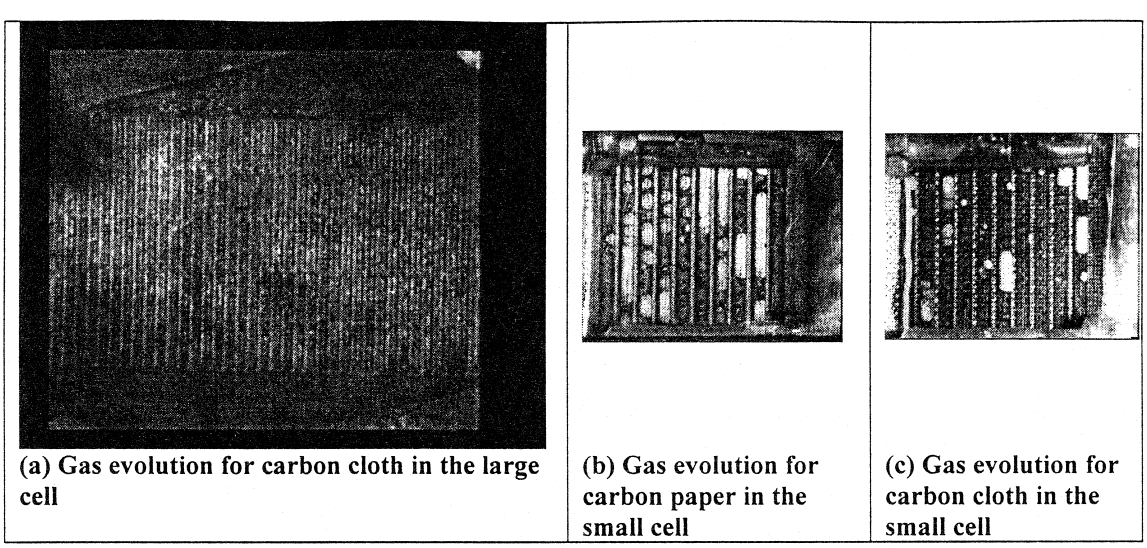

Fig. 5. Gas evolution patterns in the DMFC cells. (a) Small cell with carbon cloth, (b) small cell with carbon paper, (c) large cell with carbon cloth. 30 mA cm^{-2}, 75°C, 206 cm^3 min^{-1}.

volume is practically occupied by gas slugs. The effect of increased liquid feed flow rate served to reduce the build up of gas slugs in the flow channel. As the current density is increased there is clearly an increase in the volume of gas generated and the production of large gas slugs even at high flow rates used.

The results of the flow visualisation in the small cell where gas management problems, slug and channel flow were highlighted at what were reported to be optimum flow rates for liquid feed DMFC, led to the design of an improved flow bed based on the concept of a plate heat exchanger, as shown in Fig. 1b. In the case of the large cell the use of the triangular shaped outlet section was found to be beneficial in solving the gas bubble removal problem from the flow bed to the outlet manifold. The gas is collected on the inclined edge of the section and forms a continuous fast moving gas stream. The structure of the area (spots that support the MEA and leave a large void area) does not impose a significant barrier to movement of bubbles. As the flow rate increases the width of that gas zone decreases and thus the combination of flow bed design and high flow rate gives an excellent gas removal with little noticeable gas accumulation. In the case of the large size cell we are typically in the bubble flow regime, if not for the whole cell at least for the lowest parts (Fig. 5c). It was expected that scaling up DMFC will pose significant carbon dioxide removal problems. As the active area increases the amount of gas produced increases significantly. For a large cell of 270 cm^2 (the prototype size to be used in our stack studies) operating at 100 mA cm^{-2} and 1.0 dm^3 min^{-1} liquid flow rate, the gas outlet volumetric flow rate is almost 40% of the total outlet flow rate. The present study showed that a well designed flow bed, with a relatively large exit area, could be beneficial from a gas management point of view. Overall this work demonstrated the importance of gas management in the DMFC and selection of suitable liquid flow rates. The issue of gas flow control clearly has engineering implications on heat transfer and the temperature change, the conversion of methanol, pressure drop behaviour, etc. which will occur in the DMFC on scale up.

5. Engineering parameters

The direct methanol fuel cell can be operated with either liquid methanol solution or vaporised methanol solution. The pros and cons of both types of operation are listed in Table 1. Many of the issues over suitable fuel conditions revolve around fuel utilisation and thermal management in relation to power performance.

5.1. Vapour feed or liquid feed cells

Performance tests have been performed with liquid feed and vapour feed cells under similar operating conditions with similar cells and MEAs. One of the important factors in the performance of the liquid feed direct methanol fuel cell is that the cell voltage and power densities achieved are significantly lower than those obtained with operation with a vapour feed system, with what are essentially the same operating conditions (see Fig. 6). There are several factors, which can bring about the inferior performance of the liquid feed cell:

1. mass transfer characteristics of methanol supply to the anode catalyst are inferior
2. the extent of methanol crossover from anode to cathode
3. poorer gas release at the electrocatalyst surface
4. greater localised cooling of the anode catalyst.

The implications of this performance difference are that vapour feed cells are preferred from a simple power

Table 1
Features of liquid and vapour feed DMFC

Vapour feed systems	Liquid feed systems
Advantages	
possible superior performance	good hydration of the membrane
possible higher methanol fuel conversions	easy supply of fuel
easy methanol feed recycle	simple separation of carbon dioxide gas
no gas bubble formation	higher thermal capacity for cooling and heat transfer
Disadvantages	
higher thermal requirement in fuel vaporisation	inferior cell performance
reduced scope for heat recovery	poorer liquid phase mass transfer in cloth supports
limited thermal control of the cell	methanol and water vapour in carbon dioxide exhaust gas
possible dehydration problems of the membrane	temperature limitations with liquid operation
problems in methanol recovery from anode	gas management problems
exhaust containing large amounts of water and carbon dioxide	
	gas–liquid separator required
	greater diffusion and methanol crossover through the membrane

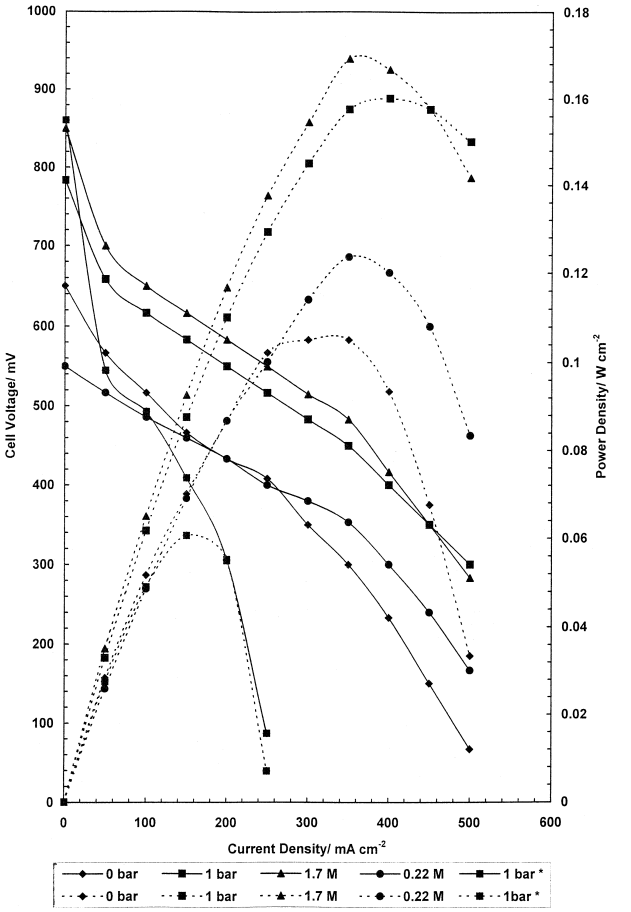

Fig. 6. Comparison of vapour feed and liquid feed performance: cell voltage (solid lines) and power density (dashed lines). ◆ 0 bar, ■ 1 bar, ▲ 1.7 M methanol, ● 0.22 M methanol. ○ liquid feed, 1 bar, 2 M methanol, 90°C cell temperature.

density performance position and that the MEA structure is not ideally suitable for liquid feed operation and redesign of the electrode assembly may be required. These issues must be considered in the wider context of cell stack and system engineering. Such engineering considerations are discussed below.

5.2. Methanol conversion and gas management

As already mentioned there is an interaction between flow rate, gas evolution and methanol conversion for liquid feed systems. The variation in methanol conversion X_{meth} and carbon dioxide gas composition at cell exit can be predicted from a simple material balance model

$$X_{\text{MeOH}} = \left[\frac{V}{\dot{Q} C_{\text{MeOH}}} \frac{\sigma l}{6F} (1 + \lambda) \right], \quad (6)$$

where, V is the cell volume, $\dot{Q}$ flow rate, C_{MeOH} inlet methanol concentration, σ the area per unit volume, and λ the methanol drag coefficient.

Fig. 7 shows the variation in methanol conversion and anode gas fraction (volume of gas to total gas and liquid volume) with current density as a function of liquid flow rate. The methanol conversions are not high (< 0.2) even at high current densities and low flow rates. However the gas fractions rise very rapidly to values in excess of 50% theoretically, which in terms of practical gas management will result in major difficulties. To maintain gas fractions below say 40%, requires flow rates typically greater than 1.0 dm^3 min^{-1} where the methanol conversion is below 0.01. High flow rates clearly will demand more energy in pumping and influence the temperature variations in the cell through a greater cooling capability.

5.3. Carbon dioxide release

The generation of a large amount of carbon dioxide gas in hot aqueous methanol solution means that on gas liquid separation there will be methanol vapour (and water

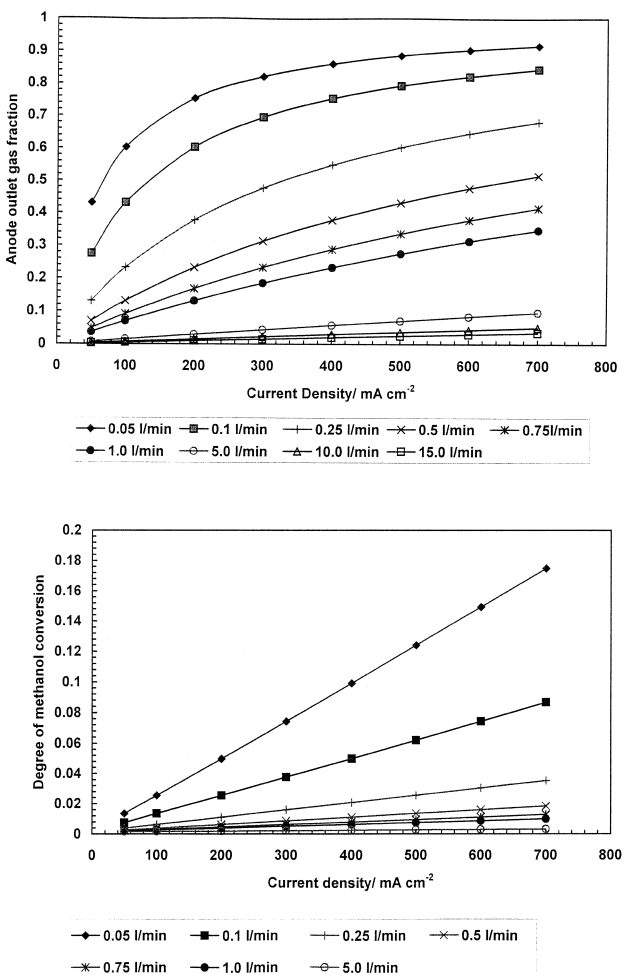

Fig. 7. Variation in methanol conversion and carbon dioxide gas fraction with current density. (a) anode gas outlet fraction; (b) methanol conversion.

vapour) present in the gas. At low current densities, and with relatively high flow rates, liquid phase operation with dissolved carbon dioxide will prevail. However under practical cell operation a two-phase operation will occur in which the methanol content in the carbon dioxide gas will be quite large, and thus methanol must be removed before the carbon dioxide is exhausted to atmosphere.

The amount of methanol vaporised will depend upon the rate of transfer into the gas phase, but, with relatively small bubbles and large gas residence times in the liquid, an equilibrium situation will be approached. Fig. 8 shows typical predicted compositions of methanol and water in the carbon dioxide gas as a function of temperature. The vapour–liquid equilibria data was generated using the equilibrium model described in Appendix A. Clearly, it is evident that the methanol content can be very large at practical operating temperatures and ideally the majority of it should be recovered to maximise fuel efficiency. Methanol mole fraction in the gas can vary between 0.1 and 0.35 at temperatures around 90°C depending upon the methanol concentration at the cell outlet. This exit concentration of methanol in the liquid should clearly be minimised to reduce the methanol vaporisation losses but, as we saw in Fig. 7, the degree of conversion of methanol in the liquid is relatively small to maintain moderate gas fractions of carbon dioxide. In addition power performance is particularly influenced by methanol concentration which should not ideally fall much below 1.0 M for acceptable performance.

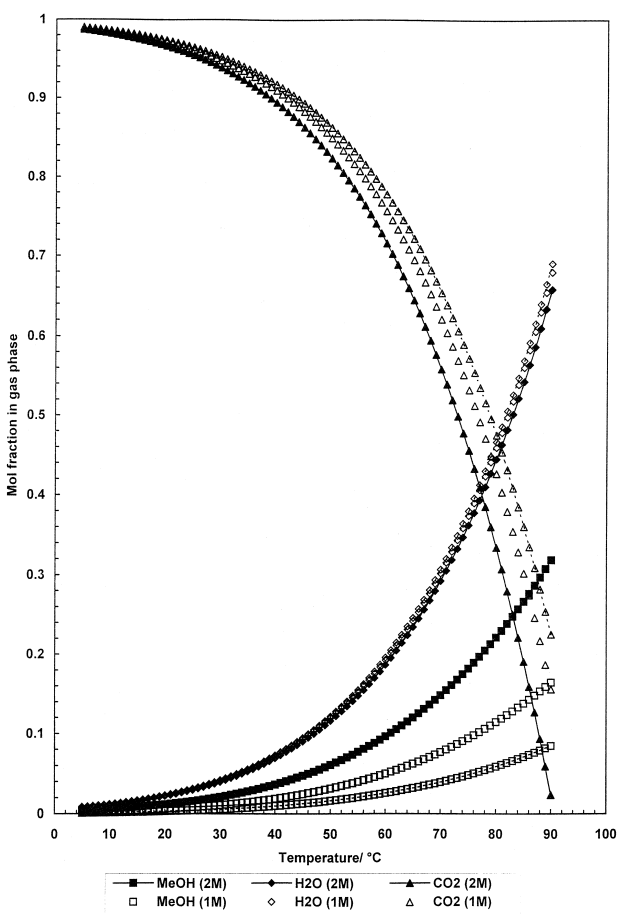

Fig. 8. Vapour–liquid equilibrium of methanol and water in the anode exhaust gas (anode side pressure 1 bar).

Several potential methods exist for the removal of the methanol from the carbon dioxide and include:

1. condensation
2. catalytic combustion
3. electrocatalytic combustion
4. vapour phase separation by, e.g., adsorption, absorption, membranes.

Of these catalytic combustion may be cheaper, but gives little return in terms of energy recovery and thus may be applicable only when the methanol content in the vapour is relatively low.

5.4. Condensation of methanol

The use of condensation to recover methanol from the carbon dioxide gas is, in principle, relatively straightforward. However, condensation in the presence of large amounts of non-condensables requires considerable efforts when near complete condensation is required, i.e., when the composition of the condensing liquid is virtually equal to that of the exit vapour from the condenser. Such a situation will require significant reduction in temperature (and/or pressure) to be effective. This is readily apparent from the vapour liquid equilibrium data of Fig. 8 where, even at low temperature, there remains a few percent of methanol in the carbon dioxide.

The performance of the condenser has been determined from a simple condenser model described in Appendix A. A realistic (perhaps optimistic) requirement for the condenser is the gas outlet temperature of 20°C. If we assume that the methanol solution fuel cell stack inlet concentration is 2 M and that the gas phase outlet temperature is 90°C, then the methanol content is approximately 35%. According to our calculations the maximum amount of methanol that is stripped away as a proportion of methanol feed to the cell is around 6% (at 700 mA cm^{-2}, 1 bar anode side pressure, a 25 cell stack of 272 cm^2 active area per cell). After the condenser this quantity falls to 2.3% (20°C condenser outlet temperature, 1 bar condenser outlet pressure). This will give an almost 60% recovery in the amount of methanol that is removed from the gas phase, but means that the carbon dioxide gas still contains substantial quantities of methanol (13%). In addition, to maximise the methanol recovered, the requirements of the heat exchanger must also be considered.

Fig. 9 shows the total required heat duty from a condenser for a 25 cell stack of 272 cm^2 active area per cell and for a range of current densities (50–700 mA cm^{-2}). In

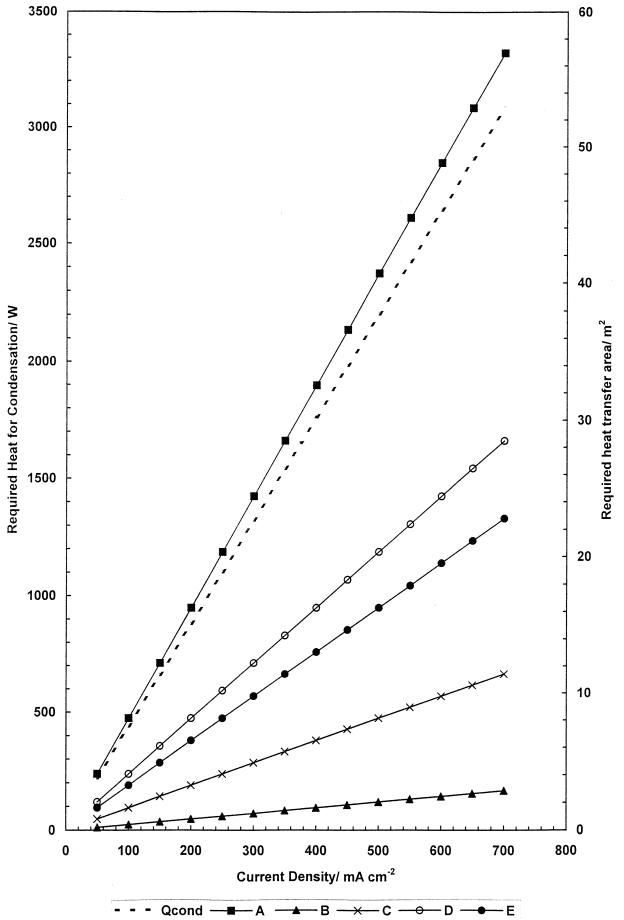

Fig. 9. Variation of heat transfer areas and heat load for the condensation of the exhaust carbon dioxide stream. Case A: An air cooled shell and tube heat exchanger ($h = 30$ W m^{-2} K^{-1}). Case B: A water cooled shell and tube heat exchanger for vapour condensation ($h = 400$ W m^{-2} K^{-1}). Case C: A water cooled finned heat exchanger ($h = 100$ W m^{-2} K^{-1}). Case D: A water cooled spiral type heat exchanger ($h = 40$ W m^{-2} K^{-1}). Case E: A water cooled shell and tube heat exchanger ($h = 50$ W m^{-2} K^{-1}).

the same graph we present estimations (solid lines) of the required heat transfer area from various type of condensers. The two different coolants (water and air) define the three options for the fuel cell stack designer: (1) use the anode inlet feed for cooling the gas and preheating prior to its entrance in the cell (i.e., heat retrieval), with the penalty that this stream is already at an elevated temperature; (2) use of air or the cathode inlet stream (cold air) with the disadvantage of the lower heat transfer coefficients (i.e., higher heat transfer area is required); and (3) use of cooling water from a water supply: probably the best option for stationary system but with two drawbacks: (i) no heat retrieval, and (ii) not a feasible solution in the case of vehicular applications.

It is apparent, in the data of Fig. 9, that significant heat transfer area is required using fairly conventional heat exchangers. Even if more compact heat exchangers with greater heat transfer coefficients were researched the cost and engineering of this is not insignificant.

It is clear, from the preliminary estimations, that for a practical fuel cell operation the carbon dioxide exhaust gas will, even after condensation, contain significant amounts of methanol vapour. This gas–vapour cannot be exhausted to atmosphere without further treatment. One option for this further treatment is to attempt electrocatalytic combustion and recover energy from the methanol.

5.5. Electrocatalytic combustion of methanol vapour

In order to assess the feasibility of electrocatalytic combustion of methanol we operated our fuel cells in the gas–vapour phase. This was achieved by bubbling nitrogen through methanol solutions, contained in a simple reservoir, prior to feeding to the fuel cell. This was designed to simulate the ‘saturation’ of carbon dioxide with methanol and water. Fig. 10a shows the performance of the DMFC with nitrogen and methanol vapour produced from solutions containing 0.11 to 0.33 M using catalyst provided by Johnson Matthey. The cell operation is clearly possible although performance is lower than that experienced with the liquid feed operation. The feasibility of this approach

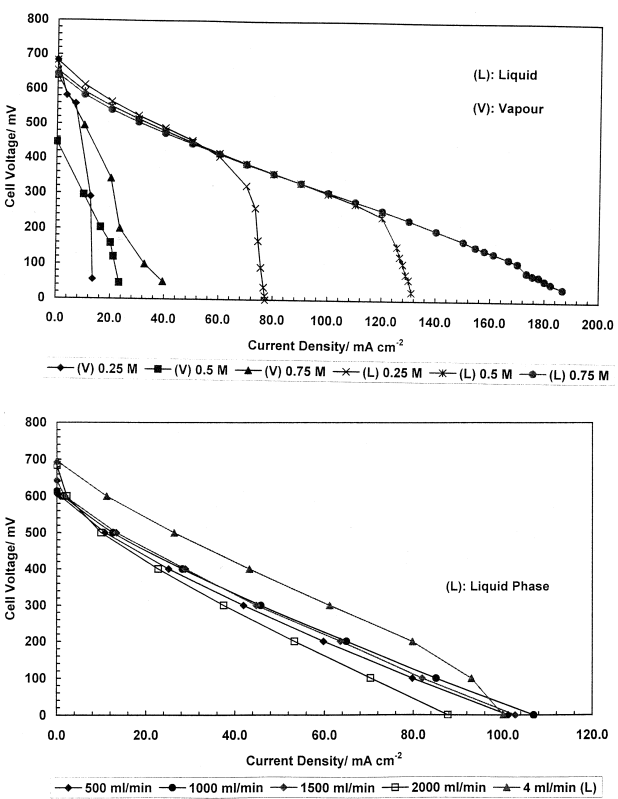

Fig. 10. Cell voltage performance of the DMFC with methanol ‘saturated’ nitrogen of operation. (a) Low liquid sump composition at 90°C. (b) liquid methanol sump concentration 2 M, 75°C.

depends on the conditions of operation and the actual content of methanol in the vapour. In our tests there is some uncertainty as to the whether the equilibrium methanol vapour composition was actually achieved due to the relatively short residence time in comparison to that in a fuel cell stack. We also investigated the operation of the vapour fed cell with a feed produced from vaporising a 2.0 M solution of methanol. The data shown in Fig. 10b, at different flow rates of gas, show quite good cell voltage performance for a liquid feed at 75°C, and are sufficiently encouraging in comparison to the liquid feed data. Further work in this area is required to 'optimise' operation, although the feasibility of the approach has been demonstrated. In addition, some consideration as to the water content in the vapour phase must be made with respect to methanol combustion and membrane hydration.

5.6. Vapour feed operation

In view of the potential engineering problems associated with liquid feed operation and the above-demonstrated operation of the DMFC with low concentrations of methanol in the vapour phase, it is informative to consider further the operation of vapour feed cells. Fig. 6 shows typical performance of the vapour feed and liquid feed operation using identical MEAs produced using the in house Newcastle catalyst. It is clear that the vapour feed cells are capable of a better performance, even at relatively low vapour phase concentrations of methanol. An attraction of vapour feed operation is that problems associated with carbon dioxide bubble generation are non-existent and also that higher temperature of operation are possible. Using vaporised dilute solutions of methanol (<2 M) results in only small volume changes in the gas during reaction, and thus only small changes in volumetric flow and methanol residence time. For example, for 1.0 mol reaction of methanol, the consumption of water by reaction and by electro-osmosis across the membrane is of the order of 4 mol (assuming a water drag coefficient of approximately 3). Thus the net change in moles in the vapour (remembering that 1 mol methanol produces 1 mol carbon dioxide) is 4.0 from a solution containing approximately 56 mol and thus a reduction in molar content is approximately 7%. Thus, sufficient water will be present in the system to maintain electrical performance, although the issue of temperature change in the cell and fluid should be considered.

For vapour fed operation a plug flow model in the anode is a suitable approximation and the variation in mole fraction y_{me} is given by

$$\frac{y_{\mathrm{MeOH}}}{y_{\mathrm{MeOH,o}}} = \mathrm{e}^{-kr}, \tag{7}$$

where y_{MeOH} is the inlet mol fraction of methanol in the vapour, τ is the residence time based on the channel volume, and

$$k = \frac{ISRT}{6FPV_{\mathrm{channel}}}, \tag{8}$$

where I is the current density, S is the cross-sectional area, P is the total pressure, and V_{channel} is the volume of the cell channels.

For the cell stack system at Newcastle: $k = 3.26 \times 10^{-5} I$, at 90°C, channel depth 2 mm, 1 bar anode pressure.

It has been demonstrated that operation of vapour feed cells can be achieved with reasonable power performance using a vaporised 0.2 M methanol solution (see Fig. 6). For a 90% methanol vapour conversion (2 to 0.2 M) the variation in residence time can be seen in Fig. 11, which is a plot of Eq. (4) above. The residence time is typically less than 100 s which is not large but has other implications in terms of cell operation. The cell performance depends on controlling the temperature of operation, which is influenced by the vapour flow rate and conversion as well as current density. If we assume initially that the cell is a

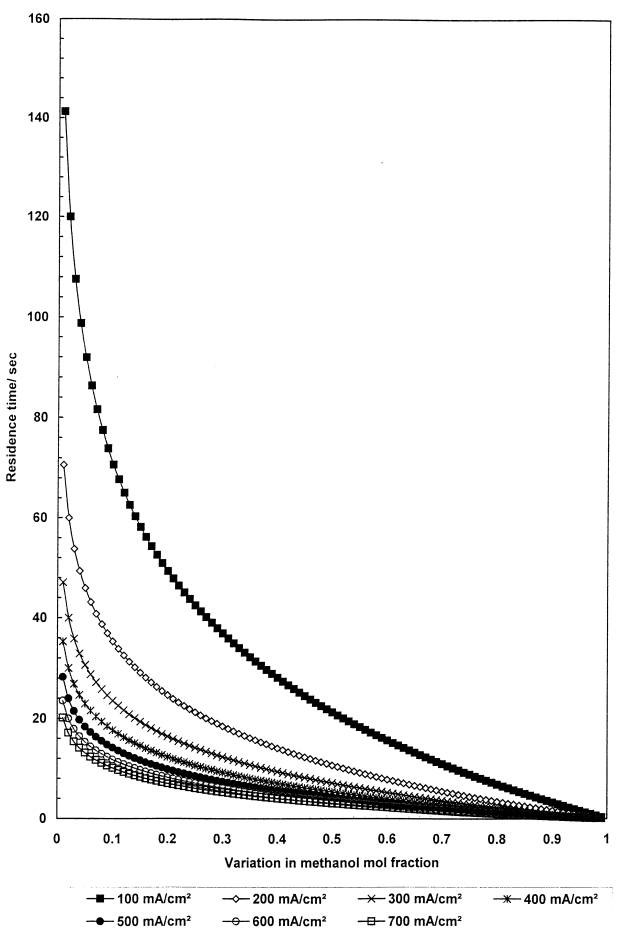

Fig. 11. Variation of methanol mole fraction with residence time for vapour feed operation.

'black box' at temperature T_c, then the operating temperature is essentially determined by the stack external heat transfer and the convective heat transfer to the fluids (fuel and oxidant). The temperature change of the methanol vapour, ΔT, is obtained from a simple heat balance

$$hA\Delta T_{ln} = Q\rho C_p \Delta T, \quad (9)$$

assuming that the density and heat capacity remain constant.

The exit vapour temperature predicted must clearly be lower than the cell stack temperature which will depend on many operating parameters and is the subject of a much more detailed modelling.

Even assuming a high, say 90%, conversion of methanol vapour is possible, there will still be a significant quantity of methanol in the vapour from the stack. Recovery of the methanol by condensation may be partly effective, although again limitations in practical conditions will mean

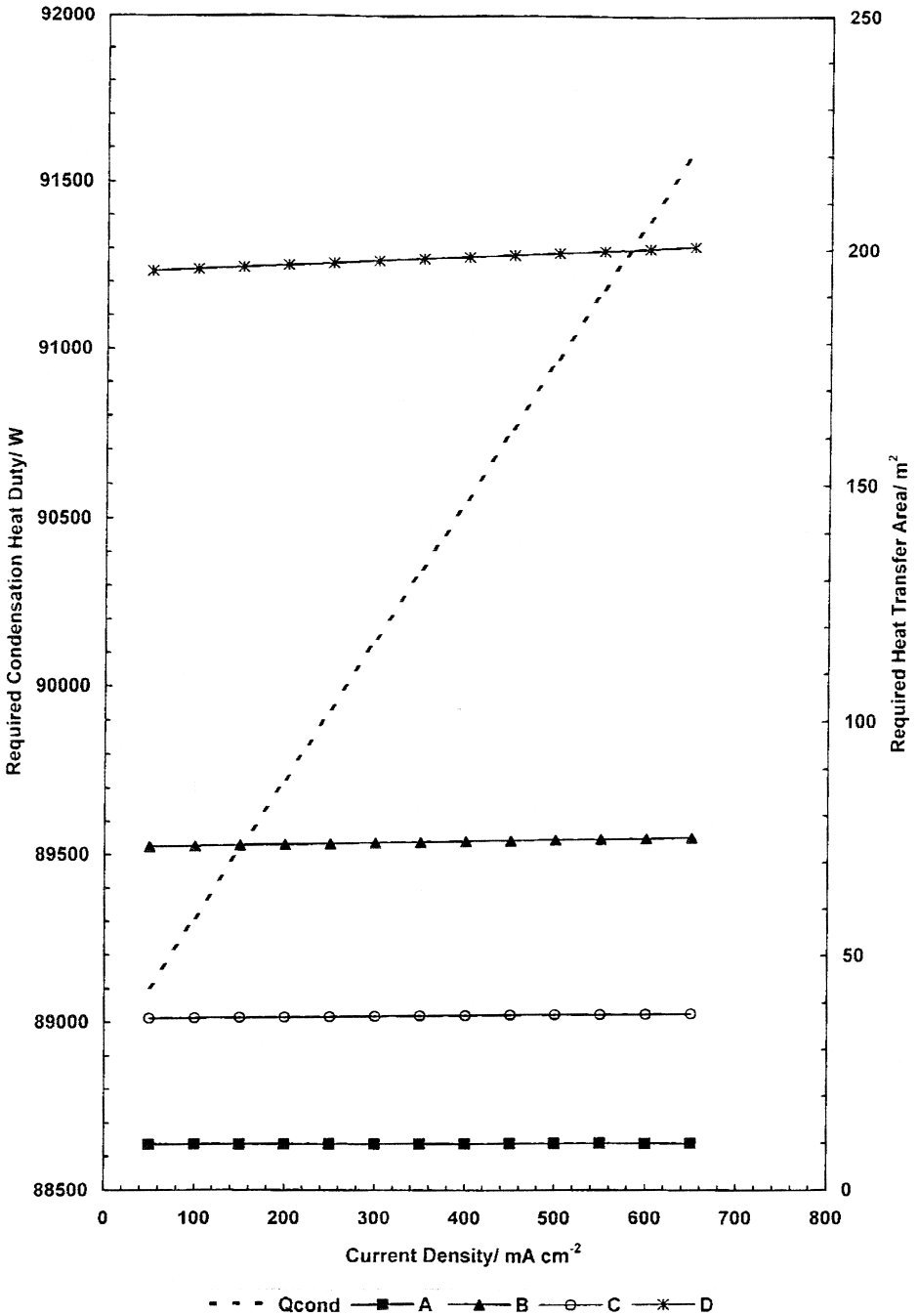

Fig. 12. Variation of heat transfer areas and heat load for the condensation of the exhaust stream for vapour feed operation. Case A: A water cooled shell and tube heat exchanger for vapour condensation ($h = 3000$ W/m^{2}K). Case B: A water cooled shell and tube heat exchanger for organic solvent vapour condensation ($h = 400$ W/m^{2}K). Case C: A water cooled shell and tube heat exchanger for low boiling hydrocarbons vapour condensation ($h = 800$ W/m^{2}K). Case D: A gas cooled shell and tube heat exchanger for vapour condensation ($h = 150$ W/m^{2}K).

some methanol is present in the gas. We have repeated the calculations, for the liquid feed system, for the case of the vapour feed DMFC operating at 120°C with the remaining conditions the same. Fig. 12 shows the total required heat duty from the condenser for a 25 cell stack of 272 cm^2 active area per cell and for a range of current densities (50–700 mA cm^{-2}). In the same graph we present estimations (solid lines) of the required heat transfer area for various type of condensers. The heat transfer areas are quite large at least 10 m^2, and indicate the need to use a compact heat exchanger. The outlet gas from the condenser still contains some methanol in equilibrium with the liquid, although at a temperature of 20°C this is relatively small, 0.1% by volume in the exhaust gas from the condenser. The advantage of vapour feed cells with a low mol fraction of methanol in the exhaust gas (i.e., 0.4 to 2%) is that the presence of the water as the majority condensable phase favours removal of methanol and high heat transfer rates.

6. Conclusions

This work has attempted to address some of the important engineering issues associated with the design and operation of DMFC stack systems. In the liquid feed cells it has been demonstrated that there are problems associated with methanol mass transfer to the anode and carbon dioxide gas release, that significantly influence performance. The use of vapour feed cells gives a superior power density performance and avoids the problems associated with methanol stripping from the feed due to carbon dioxide generation. The recovery of methanol from the exhaust gas is not readily achieved by simple condensation. An alternative to condensation (or used with condensation) to remove the methanol is required, e.g., molecular sieves. Alternatively, carbon dioxide gas can be removed form the exhaust vapour with the gas–vapour stream recycled to the cell stack, with methanol and water vapour added to maintain the required stack operating concentrations.

The use of electrocatalytic combustion of the methanol in the carbon dioxide methanol vapour is an option which is at least electrochemically viable. This may lead to a system design which uses both liquid feed and vapour feed cells. At the moment, many questions remain unanswered as to the design and optimisation of DMFC stack systems until performance data is obtained on large scale cells. However, it should also be noted that many of the problems associated with the anode side of the DMFC are duplicated with the cathode side as long as the problem of methanol crossover exists.

Acknowledgements

The authors would like to acknowledge the following for support of this research: (1) The EPSRC for support of Dr. W.M. Taama. (2) The European Commission for a TMR Marie Curie research training grant to Mr. P. Argyropoulos. (3) Johnson Matthey Technology Centre for the supply of catalyst.

Appendix A

A.1. Vapour pressure calculation methodology

This appendix presents the calculation methodology for estimating the water and methanol saturation content of the anode side gas-phase at the anode side mean temperature and pressure conditions. The cell is assumed to contain liquid water over its cross-section, and the water vapour pressure is assumed for simplicity to obey:

$$p_{H_2O} = y_{H_2O,v} P_{anode} = y_{H_2O,l} p^s_{H_2O}, \quad (A1)$$

where $y_{H_2O,v}$ is the mole fraction of water vapour in the cathode side flow bed, $y_{H_2O,l}$ is the liquid phase mole fraction which is a function of methanol concentration, and $P^s_{H_2O}$ is the vapour pressure of pure water which is a function of temperature. The mole fraction of water is given by:

$$y_{H_2O} = \frac{p^s_{H_2O}(T)}{p_{anode}}, \quad (A2)$$

where $P^s_{H2O}(T)$, in Pa, is calculated according to Wagner equation [13] as:

$$\ln\left(\frac{p^s_{H_2O}}{P_{c,H_2O}}\right) = \left[\left(\frac{1}{1-x_{H_2O}}\right)\left(-7.76451\,x_{H_2O} + 1.45838\,x^{1.5}_{H_2O} - 2.77580\,x^3_{H_2O} - 1.23303\,x^6_{H_2O}\right)\right] \quad (A3)$$

where

$$x_{H_2O} = \left(1 - \frac{T}{T_{c,H_2O}}\right), \quad (A4)$$

T_{c,H_2O} is the water critical temperature (647.3 K) and P_{c,H_2O} is the water critical pressure (221.2 bar).

The air is also saturated with methanol, which obeys Dalton's and Raoult's laws:

$$p_{MeOH} = y_{MeOH,v} P_{anode} = y_{MeOH,l} p^s_{MeOH}, \quad (A5)$$

where $y_{MeOH,v}$ is the mole fraction of methanol vapour in the cathode side flow bed, $y_{MeOH,l}$ is the liquid phase mole fraction which is only a function of the methanol concen-

Table 2
Correlating constants for activity coefficients at infinite dilution

Solute	Solvent	T (°C)	α	ε	ζ	θ	N_1	N_2
MeOH	H_2O	25	−0.995	0.622	0.558	–	1	–
		60	−0.755	0.583	0.460	–	1	–
		100	−0.420	0.517	0.230	–	1	–
H_2O	MeOH	25	0.760	–	–	−0.630	–	1
		60	0.680	–	–	−0.440	–	1
		100	0.617	–	–	−0.280	–	1

tration, and p^s_{MeOH} is the vapour pressure of pure methanol which is a function of temperature.

Methanol vapour pressure can be calculated again with the aid of the Wagner equation:

$$\ln\left(\frac{p^s_{MeOH}}{P_{c,MeOH}}\right) = \left[\left(\frac{1}{1-x_{MeOH}}\right)\left(-8.54796\,x_{MeOH} + 0.76982\,x^{1.5}_{MeOH} - 3.10850\,x^{3}_{MeOH} - 1.54481\,x^{6}_{MeOH}\right)\right] \quad (A6)$$

where

$$x_{MeOH} = \left(1 - \frac{T}{T_{c,MeOH}}\right), \quad (A7)$$

$T_{c,MeOH}$ is the methanol critical temperature (512.6 K) and $P_{c,MeOH}$ the water critical pressure (80.9 bar).

A.2. Activity coefficients

Activity coefficients can be calculated with the aid of van Laar equation [13]:

$$g^E = A x_{MeOH}\, x_{H_2O}\left(x_{MeOH}\frac{A}{B} + x_{H_2O}\right)^{-1}, \quad (A8)$$

where A and B can be calculated as:

$$A = RT \ln \gamma^{\infty}_{MeOH}, \quad (A9)$$

$$B = RT \ln \gamma^{\infty}_{H_2O}, \quad (A10)$$

and hence:

$$\ln \gamma_{MeOH} = \frac{A\left(1 + \frac{A}{B}\frac{x_{MeOH}}{x_{H_2O}}\right)^{-2}}{RT}, \quad (A11)$$

$$\ln \gamma_{H_2O} = \frac{B\left(1 + \frac{B}{A}\frac{x_{H_2O}}{x_{MeOH}}\right)^{-2}}{RT}, \quad (A12)$$

The only unknowns are the quantities γ^{∞}_{MeOH} and $\gamma^{\infty}_{H_2O}$ which represent activity coefficients for a binary mixture at infinite dilution. According to Reid [13] the value of this two parameters can be calculated according to the formula:

$$\log \gamma^{\infty}_j = a + \varepsilon N_1 + \frac{\zeta}{N_1} + \frac{\theta}{N_2}. \quad (A13)$$

Values of the adjustable parameters for the binary mixture of MeOH/H_2O are presented in Table 2.

A.3. Enthalpy of vaporisation

The enthalpy of vaporisation, ΔH_v, can be related to temperature T, T_r the ratio between the actual temperature and the critical temperature, and ω the acentric factor [13]:

$$\frac{\Delta H_v}{RT_c} = 7.08(1 - T_r)^{0.354} + 10.95\omega(1 - T_r)^{0.456}, \quad (A14)$$

which is valid for $0.5 < T_r < 0.7$.

Table 3 shows the values of the two parameters T_c and ω needed to calculate the enthalpy of vaporisation for methanol and water.

A.4. Mass balances in the cell / stack outlet

Initially the mass rate of carbon dioxide gas produced is a direct function of the current density:

$$\dot{m}_{CO_2,out} = \frac{A_{active} \times MW_{CO_2} \times j \times s_{CO_2}}{100 \times ne \times F} \quad (A15)$$

where A_{active} is the active area of the cell, MW is the molar mass and s is the stoichiometric coefficient.

Hence the moles of carbon dioxide at the cell outlet is also known:

$$\dot{n}_{CO_2,out} = \frac{A_{active} \times j \times s_{CO_2}}{100 \times ne \times F}. \quad (A16)$$

The temperature and the pressure at the cell outlet are known and if we assume that the solution concentration has not altered significantly from the inlet, we are able to calculate the amount of water and methanol in the gaseous phase. Since the ratio between the water and methanol moles and the carbon dioxide moles with the water–methanol moles are also known, we are able to estimate the mass of water and methanol at the gaseous phase.

At the outlet of the anode flow bed plate the inlet volume of aqueous methanol solution is reduced by the

Table 3
Critical temperature and acentric factor for water and methanol

	T_c	ω
MeOH	512.6	0.556
H_2O	647.3	0.344

amount of methanol consumed by electrochemical reaction plus the methanol transferred across the membrane by electro-osmosis, i.e., the methanol crossover, plus the amount of methanol that is vaporised:

$$\dot{m}_{\mathrm{MeOH,out}} = \left(\dot{Q}_{\mathrm{i}} \times C_{\mathrm{MeOH}} \times \mathrm{MW}_{\mathrm{MeOH}}\right) - \frac{s_{\mathrm{MeOH}} \times j \times A_{\mathrm{active}} \times \mathrm{MW}_{\mathrm{MeOH}}}{100 \times ne \times F} - \frac{x_{\mathrm{drag,MeOH}} \times j \times A_{\mathrm{active}} \times \mathrm{MW}_{\mathrm{MeOH}}}{100 \times n \times F} - m_{\mathrm{MeOH,vapourised}}, \quad (A17)$$

where Q is the volumetric flow rate, x the mole fraction and C the concentration.

The electrochemical reaction also consumes water (1 mol methanol/mol water) which is in the methanol aqueous solution. Furthermore for each proton produced by the electrochemical reaction and transferred to the cathode through the Nafion membrane, approximately 2.5 molecules of water are dragged by electro-osmosis. Hence the total quantity of water removed from the anode stream is:

$$\dot{m}_{\mathrm{H_2O,out}} = \dot{Q}_{\mathrm{i}}\,\rho_{\mathrm{H_2O}}\left(1 - \left(\frac{\dot{Q}_{\mathrm{i}} \times C_{\mathrm{MeOH}} \times \mathrm{MW}_{\mathrm{MeOH}}}{\rho_{\mathrm{MeOH}}}\right)\right) - \frac{s_{\mathrm{H_2O}} \times j \times A_{\mathrm{mea}} \times \mathrm{MW}_{\mathrm{H_2O}}}{100 \times ne \times F} - \frac{x_{\mathrm{drag,H_2O}} \times j \times A_{\mathrm{mea}} \times \mathrm{MW}_{\mathrm{H_2O}}}{100 \times n \times F} - m_{\mathrm{H_2O,vapourised}} \quad (A18)$$

In accordance with the above-calculated quantities the mass fractions at the outlet of each cell are:

$$x_{\mathrm{H_2O}} = \frac{\dot{m}_{\mathrm{H_2O_2,out}}}{\dot{m}_{\mathrm{MeOH,out}} + \dot{m}_{\mathrm{H_2O,out}}}, \quad (A19)$$

$$x_{\mathrm{MeOH}} = \frac{\dot{m}_{\mathrm{MeOH,out}}}{\dot{m}_{\mathrm{MeOH,out}} + \dot{m}_{\mathrm{H_2O,out}}}, \quad (A20)$$

A.5. Mass balances at the gaseous phase condenser

Assuming a well-mixed ternary system of MeOH/H_2O/CO_2 we can formulate the following material balance over the cell flow bed:

$$\frac{y_{\mathrm{MeOH,i}} - y_{\mathrm{MeOH}}}{y_{\mathrm{H_2O,i}} - y_{\mathrm{H_2O}}} = \frac{x_{\mathrm{MeOH}}}{1 - x_{\mathrm{MeOH}}}, \quad (A21)$$

where y refer to mole fraction in vapour phase, x to mole fraction in liquid phase and subscript 'i' denotes inlet composition. Equilibrium conditions can be approximated as:

$$y_{\mathrm{j}} = x_{\mathrm{j}}\gamma_{\mathrm{j}}\frac{p^{\mathrm{s}}_{\mathrm{j}}}{P_{\mathrm{anode}}}. \quad (A22)$$

For the ternary system (MeOH/H_2O/CO_2) the following equations are valid:

$$P_{\mathrm{anode}} = P_{\mathrm{CO_2}} + P_{\mathrm{MeOH}} + P_{\mathrm{H_2O}}, \quad (A23)$$

$$y_{\mathrm{CO_2}} + y_{\mathrm{MeOH}} + y_{\mathrm{H_2O}} = 1, \quad (A24)$$

$$x_{\mathrm{MeOH}} + x_{\mathrm{H_2O}} = 1. \quad (A25)$$

By making use of Eqs. (A22) and (A25), Eq. (A21) becomes

$$\frac{y_{\mathrm{MeOH,i}} - y_{\mathrm{MeOH}}}{y_{\mathrm{H_2O,i}} - \left(1 - \dfrac{y_{\mathrm{MeOH}}}{\gamma_{\mathrm{MeOH}}\dfrac{p^{\mathrm{s}}_{\mathrm{MeOH}}}{P_{\mathrm{anode}}}}\right)\gamma_{\mathrm{H_2O}}\dfrac{p^{\mathrm{s}}_{\mathrm{H_2O}}}{P_{\mathrm{anode}}}} = \frac{\dfrac{y_{\mathrm{MeOH}}}{\gamma_{\mathrm{MeOH}}\dfrac{p^{\mathrm{s}}_{\mathrm{MeOH}}}{P_{\mathrm{anode}}}}}{1 - \dfrac{y_{\mathrm{MeOH}}}{\gamma_{\mathrm{MeOH}}\dfrac{p^{\mathrm{s}}_{\mathrm{MeOH}}}{P_{\mathrm{anode}}}}}. \quad (A26)$$

A.6. Condenser sizing calculations

The temperature change of the gaseous phase, ΔT, is obtained from a simple heat balance

$$hA\Delta T_{\mathrm{ln}} = \dot{Q}\rho C_{\mathrm{p}}\Delta T + \Delta H_{\mathrm{v}}, \quad (A27)$$

where

$$\Delta T = (T_{\mathrm{out}} - T_{\mathrm{in}}), \quad (A28)$$

which is the temperature difference between the inlet and the outlet of the condenser and ΔT_{ln} is the logarithmic mean temperature:

$$\Delta T_{\mathrm{ln}} = \ln\left(\frac{T_{\mathrm{out}} - T_{\mathrm{w}}}{T_{\mathrm{in}} - T_{\mathrm{w}}}\right). \quad (A29)$$

References

[1] J.M. Leger, C. Lamy, Berichte Der Bunsen-Gesellschaft fur Physikalische Chemie 94 (9) (1990) 1021–1025.
[2] D.S. Cameron, G.A. Hards, B. Harrison, R.J. Potter, Platinum Metals Review 31 (4) (1987) 173–181.
[3] G.L. Troughton, A. Hamnett, Bull. Electrochem. 7 (1991) 488.
[4] K. Scott, W.M. Taama, J. Cruickshank, J. Power Sources 65 (1997) 159.

[5] S.R. Narayanan, G. Halpert, W. Chum, B. Jeffries-Nakamura, T.I. Valdez, H. Frank, S. Surampudi, Proceedings of the Power Sources Conference, Cherry Hill, NJ, USA, 1996.
[6] M.K. Ravikumar, A.K. Shukla, J. Electrochem. Soc. 143 (1996) 2601.
[7] S. Surampudi, S.R. Narayanan, E. Vamos, H. Frank, G. Halpert, A. LaConti, J. Kosek, G.K. SuryaPakash, G.A. Olah, J. Power Sources 47 (1994) 377.
[8] T.I. Valdez, S.R. Narayanan, H. Frank, W. Chun, Proceedings of the 12th Annual Battery Conference on Applications and Advances, 1997, p. 239.
[9] J.S. Wainwright, J.T. Weng, R.F. Savinell, M. Litt, J. Electrochem. Soc. 142 (1995) L121.
[10] Direct Methanol Fuel Cell Review Meeting, Dept. of Energy and Advanced Research Projects Agency, Baltimore, April 26–27, 1994, Executive Summary.
[11] K. Scott, W.M. Taama, P. Argyropoulos, 1998 I Chem. E. Research Event, Newcastle upon Tyne, March 1998.
[12] K. Scott, W.M. Taama, P. Argyropoulos, Submitted to J. Power Sources.
[13] R.C. Reid, J.M. Prausnitz, B.E. Poling, The Properties of Gases and Liquids, 4th edn., McGraw Hill, New York, 1987.